
An RNA interference therapeutic potentially achieves functional cure of chronic hepatitis B virus infection

Received: 23 June 2025

Accepted: 18 November 2025

Cite this article as: Huang, Z.-A., Yang, Y., Yang, S. *et al.* An RNA interference therapeutic potentially achieves functional cure of chronic hepatitis B virus infection. *Nat Commun* (2025). <https://doi.org/10.1038/s41467-025-66876-5>

Ze-Ao Huang, Yang Yang, Shuo Yang, Guang-Shen Ji, Rui Fu, Zhi-Kang Tian, Yu-Cheng Wu & Geng-Shen Song

We are providing an unedited version of this manuscript to give early access to its findings. Before final publication, the manuscript will undergo further editing. Please note there may be errors present which affect the content, and all legal disclaimers apply.

If this paper is publishing under a Transparent Peer Review model then Peer Review reports will publish with the final article.

An RNA interference therapeutic potentially achieves functional cure of chronic hepatitis B virus infection

Ze-Ao Huang^{1, 2, *}, Yang Yang^{1, *}, Shuo Yang^{1, *}, Guang-Shen Ji¹, Rui Fu¹, Zhi-Kang Tian¹, Yu-Cheng Wu¹ and Geng-Shen Song^{1, 2, □}

¹ Beijing Youcare Kechuang Pharmaceutical Technology Co., Ltd., Kechuang 7th Street, BDA, Beijing 100176, China.

² Hangzhou Tianlong Pharmaceutical Co., Ltd., Room 701, Building 3, Yinhai Science and Technology Innovation Center, Xiasha Subdistrict, Qiantang District, Hangzhou, Zhejiang, 310020, China

□ Corresponding author: Geng-Shen Song (songgengshen@youcareyk.com)

* These authors contributed equally: Ze-Ao Huang, Yang Yang, Shuo Yang.

Abstract

Current therapeutics for chronic hepatitis B virus (HBV) infection are insufficient due to immune exhaustion caused by high circulating hepatitis B surface antigen (HBsAg) levels. Here, an HBV S region-targeted small interfering RNA (siRNA) is reported, aiming to dramatically suppress HBsAg and provide windows for host immune restoration. This siRNA agent, called KC13-M2G2, exhibits potent antiviral efficacy against all HBV genotypes *in vitro*. Notably, in multiple mouse models, KC13-M2G2 triggers rapid and sustained loss of HBsAg and HBV DNA accompanied by hepatitis B surface antibody seroconversion, outperforming the clinical drug elebsiran and

bepirovirsen. Toxicity studies in Sprague-Dawley rats and cynomolgus monkeys indicate satisfactory biosafety profiles of KC13-M2G2. Given that elebsiran and bepirovirsen have achieved a functional cure rate of no more than 20% in their clinical studies, KC13-M2G2 as a more potent candidate drug is expected to exhibit superior performance in clinical applications.

Introduction

Chronic hepatitis B virus (HBV) infection affects about 296 million people worldwide, and it is the primary cause of cirrhosis and hepatocellular carcinoma (HCC)¹⁻³. HBV genome is a compact 3.2 kb circular, partially double-stranded, relaxed circular DNA (rcDNA). Once entering the nucleus, HBV rcDNA is converted by endogenous enzymes into covalently closed circular DNA (cccDNA), which encodes polymerase, pre-genomic RNA, and four viral antigens, including the core antigen (HBcAg), surface antigen (HBsAg), e antigen (HBeAg), and X protein (HBx)^{4,5}. Furthermore, HBV is a highly variable virus. It includes 8 major HBV genotypes (A to H) and 2 minor genotypes (I and J) which are classified according to at least 7.5% nucleotide divergence across the complete genome⁴.

In chronic hepatitis B (CHB) virus infection, cccDNA persists in the nucleus of hepatocytes and drives viral replication. In addition, the double-stranded linear DNA formed during viral life cycle can randomly integrate into the host genome at sites of DNA breaks⁶. This integrated HBV DNA is unable to produce progeny virus, but produces massive non-infectious viral protein particles that contain HBsAg⁷. High circulatory level of the HBsAg particles can protect virus from recognition by immune system and the excessive immune stimulation results in T cell and B cell exhaustion,

leading to liver fibrosis, cirrhosis and cancer⁸⁻¹¹. As delineated in the latest expert consensus on CHB treatment navigation, reduction of the circulatory HBsAg to an undetectable level will allow reawakening of the dysfunctional immune system in the host¹². And the patients with hepatitis B surface antibody (HBsAb) seroconversion are more likely to achieve functional cure and low risk of recurrence, indicating successful restoration of HBV-specific immune responses¹². Clinical data also revealed that HBsAg loss is strongly associated with a reduced risk of long-term adverse clinical outcomes in CHB patients¹³.

Although novel therapeutics have been constantly developed, current clinical treatment of CHB is still limited to nucleos(t)ide analogs (NAs) and pegylated-interferon- α (IFN- α)^{14,15}. NAs can suppress HBV replication but generally requires lifelong therapy and cannot improve the rate of HBsAg loss. IFN- α can enhance innate antiviral response by activating interferon-stimulated genes suppressed by HBV^{16,17}, but it is limited by poor tolerability. Furthermore, young children with CHB may derive greater benefit from current IFN- α and NAs treatments than those adult patients^{18,19}.

The novel therapeutics can be classified into immunomodulators and direct antiviral agents. Immunomodulators, such as toll-like receptor agonists, therapeutic vaccines, immune checkpoint inhibitors and chimeric antigen receptor T cells, are more appropriately applied when HBsAg levels have been suppressed^{11,12}. Small interfering RNA (siRNA) and antisense oligonucleotide (ASO) are two types of direct antiviral agents, and considered as attractive therapeutics to achieve functional cure of CHB. To date, several siRNA agents have entered phase 2 trials, such as elebsiran²⁰, imdusiran²¹, xalnesiran²², Daplusiran/Tomligisiran²³. With monotherapy, these siRNA

agents hardly resulted in HBsAg loss or seroconversion in CHB patients, thus combination therapy with immunomodulators are the main clinical treatment strategies. Approximately 15% patients achieved HBsAg loss at 24-week post-treatment and most of them had a lower baseline HBsAg, (i.e., <1000 IU/mL)²⁰. There are the same concerns about the ASO agent bepirovirsen, which resulted in approximately 10% functional cure rate at 24-week post-treatment²⁴. Functional cure rates achieved by current siRNA or ASO agents are still far from the WHO' goal of eliminating HBV by 2030. New therapies using different agents or combination strategies to achieve a higher functional cure rate inclusive of patients with high HBsAg baseline are urgently needed.

In this study, an N-acetylgalactosamine (GalNAc)-conjugated siRNA (KC13-M2G2) targeting the HBV S region is developed and evaluated for efficacy in both *in vitro* and *in vivo* models. The safety profiles are investigated in both Sprague-Dawley (SD) rats and cynomolgus monkeys. KC13-M2G2 shows potential and broad antiviral efficacy against all HBV genotypes *in vitro*. Notably, KC13-M2G2 triggers rapid and sustained loss of HBsAg and HBV DNA in multiple mouse models, accompanied by hepatitis B surface antibody (HBsAb) seroconversion. KC13-M2G2 demonstrates significantly greater potency than the clinical drug elebsiran and bepirovirsen in suppression of HBsAg and induction of HBsAb seroconversion. Toxicity studies in SD rats and cynomolgus monkeys indicate satisfactory biosafety profiles of KC13-M2G2.

Results

Screening of siRNAs targeting HBV

The siRNAs targeting HBV were generated by bioinformatics methods and screening strategies²⁵.

Two rounds of screening were successively conducted for sensitive target sites and optimal modification patterns, using HepG2.2.15 cells which are stably integrated with HBV genotype D²⁶. Briefly, siRNA candidates targeting HBV were designed using publicly available algorithms, including siDirect, DSIR, DsiRNA, and sFold, based on the reference sequence NC_003977.2. A total of 26 siRNAs were manually selected according to the criterion of high target sequence conservation. The region downstream of nucleotide position 1600 was excluded from siRNA design due to its possible loss during HBV DNA integration into the host genome. The initial screening round aimed to identify sensitive target sites. All 26 siRNAs were uniformly chemically modified using the same pattern, which included the incorporation of 2'-O-methyl, 2'-fluoro and phosphorothioate modifications at specific sites to enhance siRNA stability and specificity. In addition, (E)-vinylphosphonate was introduced at the 5' end of the antisense strands to promote efficient loading into Argonaute 2. Among the 26 siRNAs, five exhibited superior anti-HBV activity compared to the others (Supplementary Fig. 1a). Based on these five lead candidates, a total of 95 siRNAs were designed by optimizing chemical modification patterns, and were subsequently evaluated in a second screening round (Supplementary Fig. 1b). Among these candidates, a total of 9 siRNAs were selected for further evaluation in rAAV-HBV mice based on a comprehensive consideration of anti-HBV efficacy and patent conflict avoidance. The selected siRNAs were conjugated with a proprietary GalNAc ligand (G1) and administered subcutaneously at a dose of 3 mg/kg once weekly for a total of three injections. The siRNAs KC13-M1G1 and KC13-M2G1, which share the same nucleotide sequence (KC13), but differ in their modification patterns (M1 vs. M2), demonstrated superior efficacy compared to the other candidates

(Supplementary Fig. 2). In a subsequent lower-dose study (0.5 mg/kg), KC13-M2G1 exhibited more potent anti-HBV activity than KC13-M1G1 (Supplementary Fig. 3). Furthermore, conjugation of KC13-M2 with an alternative GalNAc ligand (G2) led to a further enhancement of antiviral efficacy (Supplementary Fig. 4). These results established KC13-M2G2 as the most promising siRNA candidate for the treatment of HBV infection.

***In vitro* efficacy of KC13-M2G2**

The most potent siRNA KC13-M2G2 was then evaluated in detail. In HepG2.2.15 cells, KC13-M2G2 transfection resulted in a dose-dependent reduction of HBsAg, HBV DNA, HBeAg, HBV S mRNA and HBV total RNA, with no obvious cytotoxicity (Fig. 1). KC13-M2G2 showed superior antiviral efficacy than elebsiran, with IC₅₀ values of 0.03 vs. 0.07 nM for HBsAg, 0.08 vs. 0.11 nM for HBV DNA, 0.47 vs. 0.51 nM for HBeAg, 0.20 vs. 0.44 nM for HBV S mRNA, and 0.25 vs. 0.50 nM for HBV total RNA. Then, we further evaluate the efficacy of KC13-M2G2 in HBV-infected primary human hepatocytes (PHHs). As expected, KC13-M2G2 also exhibited distinct suppressions on all of the virological biomarkers with IC₅₀ values at nanomolar level (Supplementary Fig. 5).

Conservation analysis and pan-genotypic efficacy of KC13-M2G2

KC13-M2G2 siRNA target sequence is located within HBV S region. A total of 8836 HBV sequences available in HBVdb²⁷ were analyzed for conservation of this target sequence. The core region (position 2-19 of antisense strand) was conserved in ≥79.7% of HBV genotypes A to E,

which were estimated to account for 96% of global CHB infections²⁸ (Table 1). Sequence alignment revealed a mismatched base pair (C:T) with genotype F and H, and an additional mismatched base pair (C:T) with genotype F. These two mismatches locate at antisense strand position 18 and 15, respectively. However, the seed region (position 2-8 of antisense strand) was conserved in 93.9% of all HBV genotypes from A to H. Efficacies of KC13-M2G2 against all of ten HBV genotypes were evaluated later in HepG2 cells transfected with HBV 1.3-mer plasmids. Obvious suppressions of HBsAg were observed in all HBV genotypes, alongside the inhibitions of HBV DNA (Fig. 2 and Supplementary Fig. 6). The calculated IC₅₀ values of HBsAg across HBV genotypes A–J ranged from 0.0018 to 0.0209 nM (Supplementary Table 1), indicating pan-genotypic efficacy of KC13-M2G2 even at picomolar levels. The mismatches in the target sequence showed no impact on susceptibility to KC13-M2G2.

***In silico* off-target analysis and validation**

SiRNA specificity is not absolute and off-target genes silencing can occur through partially sequence complementation. Researches have showed the hepatotoxicity of siRNA was largely driven by miRNA-like off-target effect mediated by base paring with seed region of the siRNA antisense strand²⁹⁻³¹. To investigate miRNA-like off-target effect of KC13-M2G2, *in-silico* sequence analysis was conducted as shown in Supplementary Fig. 7a. We compared the antisense sequence to human refseq RNA database in NCBI BLAST. Genes with at most one mismatch in seed region and expressions in liver higher than 1 transcript per million (TPM) (HPA RNA-seq dataset, <https://www.proteinatlas.org/>) were filtered. A total of 13 potential off-target genes were

identified and following verified in hepG2.2.15 cells by RT-qPCR. No obvious down-regulations of these potential off-target genes were observed even at the highest transfection concentration of 30 nM (Supplementary Fig. 7b). We further conducted a comprehensive comparison between the antisense sequence and all human miRNAs in miRBase database. Our analysis revealed that no miRNAs showed significant sequence similarity to the antisense sequence, as evidenced by the absence of any miRNA with three or fewer mismatches.

Anti-HBV activity of KC13-M2G2 in rAAV-HBV-B, -C and -D mice

The *in vivo* anti-HBV activities of KC13-M2G2 were firstly investigated in rAAV-HBV mice. This particular animal model has been commonly used in pre-clinical studies of CHB therapeutics since it is consistent with the characteristics of persistent HBV infection and immunotolerance in patients with CHB³². The rAAV-HBV mice carrying HBV genotypes B, C, or D were established by intravenous injection of corresponding AAV particles. The rAAV-HBV-B and C mice were weekly administrated with KC13-M2G2 or elebsiran at doses of 3 mg/kg for three times. The first dosing day was defined as Day 0. Elebsiran and PBS vehicle were included as positive and negative controls, respectively. Data revealed that KC13-M2G2 effectively inhibited plasma HBsAg, HBeAg and HBV DNA in both rAAV-HBV-B and -C mice (Fig. 3a-c, f-h). Almost all animals (10/10 of rAAV-HBV-B mice and 9/10 of rAAV-HBV-C mice) attained rapid HBsAg and HBV DNA loss within the initial treatment and without rebound throughout the study (Supplementary Table 2, 3). Notably, alongside the reductions in virological biomarkers, seroconversion (HBsAb \geq 12 mIU/mL) was achieved by 8/10 of rAAV-HBV-B mice and 3/10 of

rAAV-HBV-C mice (Fig. 3d and i, Supplementary Table 2, 3). By contrast, elebsiran triggered maximum HBsAg and HBV DNA reductions on day 21 and gradually rebounded to the baseline. The rAAV-HBV-D mice received weekly subcutaneous injections of KC13-M2G2 at doses of 0.1, 0.3, 1, or 3 mg/kg for three times respectively. Elebsiran, administered as three weekly doses, was used as the positive control. Data indicated that KC13-M2G2 triggered dose-dependent decrease of virological biomarkers (Fig. 4). High rates of HBsAg and HBV DNA loss in 1 and 3 mg/kg groups revealed more prominent efficacy of KC13-M2G2 than elebsiran. At the same time, HBsAb seroconversion was also observed in mice treated with KC13-M2G2. Approximately 4-6/10 mice achieved HBsAb higher than 12 mIU/mL in 0.3, 1, or 3 mg/kg groups. RT-qPCR analysis of liver tissue at the terminal timepoint (Day 70) further revealed a dose-dependent reduction in intrahepatic HBV S RNA and total HBV RNA levels following KC13-M2G2 treatment (Supplementary Fig. 8).

In rAAV-HBV-D mice, Entecavir (ETV) and bepirovirsen were also used as positive controls. As expected, ETV only induced substantial reduction in HBV DNA level (Fig. 4). Bepirovirsen led to effective decrease in HBsAg and HBV DNA levels within treatment period. However, HBsAg and HBV DNA rebound appeared to be more prominent in bepirovirsen than elebsiran after treatment, which might be explained by the long-lasting efficacy of GalNAc-siRNA conjugate in hepatocytes. In addition, we also evaluated the efficacy of different dosing regimes (weekly or biweekly) of KC13-M2G2 or elebsiran in rAAV-HBV-D mice. The results showed that both dosing regimes were more efficacious than elebsiran in suppressing virological biomarkers and inducing HBsAb seroconversion. Mice receiving KC13-M2G2 weekly or biweekly appeared to have comparable

efficacy (Supplementary Fig. 9). Persistent efficacy of KC13-M2G2 was evaluated at single dose of 0.3, 1, 3, and 9 mg/kg. Data showed even at a lower dose of 1 mg/kg, KC13-M2G2 exhibited durable and significant inhibitions on HBsAg, as well as HBV DNA levels (Supplementary Fig. 10).

Humoral and cellular immune response evaluation

Indeed, the HBsAg loss coupled with HBsAb seroconversion was also observed in our early pilot study using the same siRNA sequence but alternative modification or GalNAc ligand (KC13-M1G1 and KC13-M2G1) (Supplementary Fig. 11a, b). In this study, to evaluate whether KC13-M2G1 could induce sustained protection from HBV re-exposure, mice were challenged with pAAV-HBV1.2 plasmids via intravenous injection on day 60. As a result, all mice maintained undetectable HBsAg level and a mild HBsAb fluctuation, while the non-treated mice had a high level of HBsAg (Supplementary Fig. 11d, e). To investigate whether sustained suppression of HBsAg would benefit HBV-specific immune response, mice received KC13-M1G1 were analyzed for immune profiles. The Elispot results showed obvious HBsAg-specific B cell responses, but minor responses for HBsAg-specific T cells (Supplementary Fig. 11f-i).

Anti-HBV activity of KC13-M2G2 in mice with high HBsAg baseline

Considering few patients with high HBsAg baseline achieved functional cure by current therapeutics, we evaluated the efficacy of KC13-M2G2 in rAAV-HBV -D mice model with higher HBsAg baseline of approximately 20000 IU/mL and longer observation period. KC13-M2G2 and

elebsiran were administered as three weekly doses of 3 mg/kg. Notably, KC13-M2G2 induced sustained suppression of both HBsAg and HBV DNA, which persisted to at least day 189 without evidence of rebound. HBsAg and HBV DNA loss were observed in 6/10 mice on day 189. Alongside with the reductions in virological biomarkers, HBsAb seroconversion was also achieved in these 6/10 mice (Fig. 5, Supplementary Table 4). In contrast, elebsiran and bepirovirsen showed inferior efficacy, in accordance with the performances described above.

Efficacy of KC13-M2G2 in HBV-transgenic mice

The efficacy of KC13-M2G2 was further evaluated in HBV-transgenic mice. This model carried 1.28-mer linearized HBV genotype A and expressed HBsAg, HBeAg and HBV DNA in serum³³. Mice were treated with weekly subcutaneous injection of KC13-M2G2 at the dose of 0.3, 1 and 3 mg/kg for three times respectively. Elebsiran, administered as three weekly doses of 3 mg/kg, was used as the positive control. The results showed that KC13-M2G2 significantly suppressed plasma HBsAg, HBeAg and HBV DNA (Fig. 6a-c). Rapid reductions in HBsAg and HBV DNA levels were observed in initial KC13-M2G2 treatment. Almost all mice (5-6/6) receiving 3 mg/kg KC13-M2G2 achieved HBsAg loss from day 14 to 42, and remained > 2 log₁₀ IU/mL reduction in HBsAg by day 70 (Fig. 6a, b). In addition, 3 mg/kg elebsiran exhibited comparable efficacy with 1 mg/kg KC13-M2G2 in the suppression of HBsAg and HBV DNA. Bepirovirsen showed an inferior suppression on all virological biomarkers than elebsiran in this evaluation system. Notably, A single dose of 3 mg/kg KC13-M2G2 could trigger a maximum 3 log₁₀ IU/mL reduction in HBsAg and up to 6/12 mice achieved HBsAg loss at the nadir (Supplementary Fig. 12).

Safety profiles of KC13-M2G2 in SD rats and cynomolgus monkeys

Safety profiles of KC13-M2G2 were assessed in 4-week repeat doses toxicity studies in SD rats, with endpoints that included survival, body weight, food consumption, clinical observation, serum chemistry, hematology, coagulation, gross pathology and microscopic observation after three doses of 50 or 200 mg/kg administered on day 0, 14, and 28. Main abnormal clinical pathology included increases total bilirubin (BIL-T) and alkaline phosphatase (ALP) on day 15 in animals receiving 200 mg/kg KC13-M2G2 (Fig. 7a-e). The KC13-M2G2-related microscopic findings were limited to minimal and/or mild vacuolation of hepatocytes and kupffer cells, which is similar to that of elebsiran (Fig. 7f and Supplementary Fig. 13). The animals can well tolerate the challenge of repeat doses of KC13-M2G2 even at the highest tested dose of 200 mg/kg (Fig. 7g). No other test article-related adverse findings were observed. The maximal tolerated dose (MTD) and no observed adverse effect level (NOAEL) of KC13-M2G2 were 200 and 50 mg/kg respectively in this evaluation system.

The safety profiles of KC13-M2G2 were further performed in cynomolgus monkeys. Similar parameters were investigated after three doses of 30, 100, or 200 mg/kg administered on day 0, 14, and 28. All animals survived to their scheduled necropsies (Day 30). No test article-related abnormal body weight, clinical pathology was observed (Fig. 8a-e, g). The microscopic observations included: basophilic Kupffer cells and hepatocytic vacuolations in the liver, increased foamy macrophages in the lymph nodes, and basophilic macrophages at injection sites (Fig. 8f and Supplementary Fig. 14). These microscopic findings were considered KC13-M2G2-related and

non-adverse after reviewed by at least two experienced pathologists. The NOAEL was considered to be the highest dose 200 mg/kg.

Immunogenicity of KC13-M2G2 in SD rats and cynomolgus monkeys

We systematically examined the immunogenicity of KC13-M2G2 in SD rats and cynomolgus monkeys. There were no KC13-M2G2-related changes in the serum levels of interleukin-2 (IL-2), interleukin-6 (IL-6), interleukin-10 (IL-10), tumor necrosis factor- α (TNF- α), and interferon- γ (IFN- γ) were observed (Supplementary Fig. 15a-e and Fig. 9a-e). The absolute number and percentages of lymphocytes and the subpopulations (total T cells, cytotoxic T cells and helper T cells) also did not show significant differences between the saline and KC13-M2G2 groups (Supplementary Fig. 15f-l and Fig. 9f-l). Although some fluctuations were noted at individual time points in some animals, these fluctuations exhibited no time- or dose-dependent trends and were thus considered to be caused by individual differences rather than KC13-M2G2 treatment.

Discussion

SiRNAs targeting HBV genome have been proved to be useful strategies for CHB treatment. Data from a current phase 2 study have demonstrated that siRNA-mediated HBsAg reduction is helpful for the HBsAb persistence and the robust neutralizing activity of HBsAb-containing serum³⁴. However, due to the limited efficacy of current anti-HBV siRNAs, the degree of HBsAg reduction was insufficient for HBV-specific immunity restoration. In this study, we showed a sufficiently effective siRNA with the potential for achieving HBsAg loss and restoring HBV-specific immunity.

HBV is a highly variable virus and there exist 10 HBV genotypes⁴. This suggests that it may be important to find a highly conserved target to guarantee siRNA's efficacy. In this study, we found that even mismatches exist, KC13-M2G2 still obviously inhibited HBsAg of HBV F and H genotypes at picomolar levels. As reported, siRNA antisense strand could be divided into four functional domains: the seed (position 2-8), central (position 9-12), supplementary (position 13-17), and tail (position 18-21) regions³⁵. Our results revealed that some mismatches in the supplementary and tail regions will not affect siRNAs' efficacy. That means perfect complementarity with position 2-12, other than 2-19, could be a more suitable criterion when designing siRNA for highly variable viruses. Or siRNA candidates could be designed based on a main virus sequence first and then evaluated for the conservation. Obviously, increased mismatches may also affect siRNAs' efficacy due to the low affinity with target sequence, thus the maximum number of mismatches allowed in position 13-21 should also be considered well.

Restoration of HBV-specific immunity is the ultimate goal to gain immune control over persistent HBV infection. Our results indicated that immune restoration was accessible after sufficient HBsAg reduction by siRNA treatment, although rare transient HBsAb emerged prior to HBsAg loss. Clinical research on combination treatment of elebsiran with BRII-179 (a VLP vaccine) also concluded that siRNA-induced HBsAg reduction may contribute to the persistence and efficacy of the humoral immunity in CHB participants receiving BRII-179³⁴. However, treatment with elebsiran alone had minimal effect on HBV-specific immunity, indicating that 1.2-2.6 log₁₀ reduction in HBsAg was insufficient to restore HBV-specific immunity³⁴. Considering over 10 times efficacy of KC13-M2G2 than elebsiran, KC13-M2G2 may give a satisfactory performance

in future clinical trials, either by monotherapy or combination with other immunomodulators. These findings also suggested that the functional cure potential of siRNA monotherapy for CHB may have been historically underestimated due to the suboptimal efficacy of earlier siRNAs. Specifically, less potent anti-HBV drugs might require stricter inclusion criteria (e.g., low HBsAg baseline) to induce HBsAg/HBV DNA loss and functional cure, which also emphasizes the importance of graded and personalized treatment strategy—a principle consistent with broader HBV therapeutic experiences and directly applicable to siRNA-based regimens³⁶.

Minor changes of HBsAg-specific T cell immune response were observed in our study. This probably because the reactivation of HBsAg-specific T cell had occurred before tissue sampling on day 56. Unlike immunotherapeutic agents which could induce strong cellular immune responses evaluated at 1 or 2 weeks post dosing^{37,38}, siRNA could not directly trigger immune responses, and it depended on the recognition of antigens by host recovered T cells. Therefore, it seemed difficult to find out the optimal time point for reactivation of cellular immune responses. In recent years, more attention has been paid to the immune profile changes in CHB patients treated with siRNA. In the clinical study of imdusiran, scientists observed that HBsAg reduction mediated by imdusiran was associated with increased activation of HBV-specific T cells and a decrease in exhausted CD8⁺ T cells³⁹. The clinical study of Daplusiran/Tomligisiran and ARC-520 also showed that siRNA-induced HBsAg suppression is associated with ameliorated T cell exhaustion⁴⁰. These findings confirm that siRNA-induced HBsAg suppression contributes to the reconstruction of host immune function.

For oligonucleotide-based therapeutics, chemical nucleotide modifications are typically

introduced to effectively prevent immunostimulation. But in the context of HBV treatment, appropriate immunostimulation will improve clinical outcomes. Recent studies have reported that bepirovirsen induced a potent innate immune response in both chronic hepatitis B patients and healthy volunteers, further confirming its immunostimulatory property⁴¹. Moreover, the clinical B-Fine study data strongly suggested that bepirovirsen triggered a humoral immune response in liver and periphery in treated patients⁴². As described above, clinical trials also demonstrated that siRNA treatment was associated with increased HBV-specific T cells³⁹. It seems there are different immunostimulatory mechanisms for ASO and siRNA drugs. Although heavily modified siRNAs are theoretically designed to eliminate immunostimulation, more experimental evidences are still needed.

We also noticed the work of another HBV S region targeted siRNA HT-101 which has exhibited stronger HBsAg suppression than elebsiran in phase 1b trials (maximum 2.09 vs $1.65 \log_{10}$ IU/mL HBsAg reduction at two 4-week interval doses of 200 mg)⁴³. The preclinical study on HT-101 showed a maximum HBsAg reduction of $1.97 \log_{10}$ IU/mL in rAAV-HBV mice at a single dose of 3 mg/kg⁴⁴, much lower than that of KC13-M2G2 ($3.21 \log_{10}$ IU/mL) at the same dosing regimen. Meanwhile, the article noted that HT-101 induced long-lasting suppression of HBsAg below the LLOQ. We noticed that the LLOQ mentioned here is $1.78 \log_{10}$ IU/mL, equal to 60.26 IU/mL, much higher than that in our study (2.5 IU/mL). High LLOQ value may overestimate the anti-HBV activity.

This study has several limitations. First, the anti-HBV activities were only evaluated in rAAV-mice and HBV-transgenic mice. Since mice could not naturally infect with HBV, HBV particles

produced in these two models are unable to spread among hepatocytes, which is different from clinical manifestations. HBV has a highly-restricted species tropism, infecting limited species including humans, chimpanzees and treeshrews. Research on chimpanzees is no longer permitted due to ethical considerations. Scientists have devoted many efforts to establishing non-human primate models of chronic HBV infection. Woolly monkeys and capuchin monkeys have been found to be naturally infected with HBV, but their highly endangered status makes them unsuitable for research⁴⁵. Exogenous expression of human sodium taurocholate co-transporting polypeptide (hNTCP) on rhesus macaque hepatocytes *in vivo* achieved only low levels of viral replication and liver dissemination^{45,46}. A stringent immunosuppression regimen enabled sustained viral replication in hNTCP rhesus macaques. However, serum virological biomarkers fell precipitously following the tapering and cessation of immunosuppression⁴⁷. Use of treeshrews is limited by accessibility of detection reagents and historical data. Chimeric liver humanized mice harbor partially humanized livers and supports the full viral life cycle. Immunocompetent liver humanized mice harbor both a humanized immune system and chimeric liver, and allows the investigation of immune-mediated disorders associated with HBV infections in the context of a full viral life-cycle. The high cost and technical difficulties pose great challenges for the availability of these two humanized models. Second, since efficacy and safety are the most critical aspects to be considered during drug development, more toxicity evaluations such as the long-term toxicity need to be performed according to the preclinical safety evaluation guidelines. Indeed, the long-term toxicity of KC13-M2G2 has already started and is ongoing. Third, although significant suppression of virological biomarkers has been achieved in this study, the combinational treatments with

immunomodulatory agents such as therapeutic vaccines and IFN- α , are still worthy to be further studied to improve clinical benefits.

In summary, we herein report KC13-M2G2, a promising siRNA agent for functional cure of CHB. In pre-clinical study, it exhibited potent and sustained elimination of HBsAg, induction of long-term HBsAb seroconversion, and satisfactory biosafety profiles in rats and cynomolgus monkeys. Based on these findings, KC13-M2G2 is expected to exhibit favorable performance in clinical applications in the future.

Methods

Study approval

All animal studies were performed in compliance with relevant local regulations and approved by the respective Institutional Animal Care and Use Committee (IACUC) of Jennio Biotech Co. Ltd. (Guangzhou, China, Approved Numbers: JENNIO-IACUC-2024-A005, JENNIO-IACUC-2024-A014, JENNIO-IACUC-2025-A002, JENNIO-IACUC-2025-A003), Vitalstar Biotechnology Co. Ltd. (Beijing, China, Approved Numbers: VST-SY-24062701, VST-SY-25022401), WuXi AppTec (Chengdu, China, Approved Number: CD20240731-Rats), and Pharmaron (Beijing) TSP (Beijing, China, Approved Numbers: 25-023, 24-471).

SiRNAs design and synthesis

Representative HBV genome sequences covering genotype A-J were used to find highly conserved target regions via CLUSTALW tools (<https://www.genome.jp/tools-bin/clustalw>). siRNAs

targeting the highly conserved regions were generated by bioinformatics methods and screening strategies²⁵. Sequence after nucleotide position 1600 of HBV genome was excluded because this fragment frequently lost when HBV DNA was integrated into host DNA. To enhance siRNA stability and specificity, chemical modifications with methoxyl groups, fluorine at 2' site hydroxyl groups, or phosphorothioates at the phosphonate backbone were placed at certain sites of the sense and antisense strands. To improve antisense strands loading into Argonaute 2, (E)-vinylphosphonate was modified at 5' end of the antisense strands. To achieve liver targeting, GalNAc conjugation was placed at the 3' end of the sense strands of siRNA. Several effective modification patterns had been designed by us and screened here for optimal combinations of sequence and modification.

All siRNAs used in this study were synthesized on a Tsingke Syn-HCY-192P synthesizer (Tsingke) using standard solid-phase oligonucleotide synthesis protocols as described previously²⁵. The 2'-O-Methyl, 2'-deoxy-2'-fluoro, 2'-O-methoxyethyl, 5'(E)-vyinylphosphonate, (S)-glycol nucleic acid phosphoramidites, and DNA amidites were purchased commercially. The GalNAc ligand was introduced at the 3' end of the sense strand of the siRNA using a functionalized solid support as described²⁵. The identity and purity of all siRNAs were confirmed using 1290 Infinity II Autoscale Preparative LC/MSD System (Agilent). The oligonucleotide sequences are provided in the accompanying Supplementary Data.

Antiviral activity evaluation in HepG2.2.15 cells

HepG2.2.15 cells (a gift from other laboratory) were cultured with Dulbecco's modified Eagle's

medium/ nutrient mixture F-12 (DMEM/F12) supplemented with 10% fetal bovine serum (FBS, ExCell), 1% penicillin-streptomycin (HyClone) and 370 µg/ml genetincn. SiRNAs were reversely transfected into the cells with lipofectamine RNAiMAX reagents (Invitrogen) at indicated concentrations. The medium was replaced with fresh medium on day 3 post-transfection. Supernatants were collected on day 6 post-transfection for virological biomarkers detection. The levels of HBsAg and HBeAg were measured using CLIA commercial Kits (Autobio) according to the manuals. Chemiluminescence was measured using a SpectraMax iD3 microplate reader (Molecular Devices), and the data were acquired with SoftMax Pro software v7.x. The HBV DNA were quantified by qPCR using TB Green Premix Ex TaqTM II (Tli RNaseH Plus) (takara). The qPCRs were performed on QuantStudio 7 Flex (Applied Biosystems) under the conditions of 30 s at 95 °C followed by 40 cycles at 95 °C for 5 s and at 60 °C for 34 s. Data acquisition was performed using the QuantStudio Real-Time PCR Software v1.7.2. The HBV standards were prepared by diluting the pAAV2-HBV1.3 plasmid (5 ng/µL) 60-fold to obtain a concentration of 1.0×10^7 copies/µL, followed by 10-fold serial dilution to generate seven gradient concentrations down to 10 copies/µL. The HBV DNA level in samples was calculated based on the standard curve. The primers are listed in Supplementary Table 5. HBV S mRNA and total RNA in cells were detected by RT-qPCR with primers as listed in Supplementary Table 5. Briefly, total RNAs were extracted from cells using EZ4001-EZ-Press 96 RNA Purification Kit (EZB) and reverse transcribed using HiScript III RT SuperMix for qPCR (+gDNA wiper) (Vazyme) according to the manuals. The qPCRs were performed using AceQ Universal U+ Probe Master Mix V2 (Vazyme) on QuantStudio 7 Flex (Applied Biosystems) under the conditions of 10 min at 95 °C followed by

40 cycles at 95 °C for 15 s and at 60 °C for 60 s. Glyceraldehyde-3-phosphate dehydrogenase (GAPDH) was used as a housekeeping control. The primers and probes are listed in Supplementary Table 5. Cell viabilities were determined using CellTiter-Glo (CTG) (Promega) or CCK-8 kit (Life-
ilab) according to the manuals. Luminescence and absorbance readings were performed on a SpectraMax iD3 reader (Molecular Devices).

Antiviral activity evaluation in PHHs

Cryopreserved PHHs (BioIVT) were cultured with DMEM supplemented with 10% FBS, 1% penicillin-streptomycin, 2% dimethylsulfoxide and other components (HEPES, L-proline, insulin, epidermal growth factor, dexamethasone, and sodium L-ascorbyl-2-phosphate) according to the manuals. PHHs were treated with certain concentrations of siRNAs by free uptake on day 0 and infected with HBV (genotype D, isolated from Hep2.2.15 cells) on day 1. Media were changed with fresh DMEM on day 2, 4, and 6. Virological biomarkers (HBsAg, HBeAg, HBV DNA, HBV S mRNA, and HBV total RNA) and cell viability were detected as described above.

Pan-genotypic efficacy evaluation in HBV-transfected HepG2 cells

HepG2 cells (ATCC: HB-8065) were cultured with RPMI-1640 medium (Gibco) supplemented with 10% FBS and 1% penicillin-streptomycin. Cells were transfected with HBV plasmids of different genotypes on day 0 using transfection agent FuGENE HD (Promega) and siRNAs on day 1 using lipofectamine RNAiMAX reagents. The medium was replaced with fresh medium on day 3 post-transfection. Supernatants were collected on day 6 post-transfection for HBsAg

quantification using CLIA commercial Kits (Autobio). HBV DNA in cells were quantified by qPCR. Briefly, the cells were harvested and lysed with 0.33% NP-40 (abcam). The DNAs were extracted from cells using QuickExtract DNA Extraction Solution (Lucigen) after treated with Turbo Dnase (Invitrogen). The qPCRs were performed using AceQ Universal U+ Probe Master Mix V2 (Vazyme) on QuantStudio 7 Flex (Applied Biosystems) under the conditions of 10 min at 95 °C followed by 40 cycles at 95 °C for 15 s and at 60 °C for 60 s. The HBV standards were prepared as described above.

Off-target effect evaluation

A combination of *in silico* bioinformatics methods and *in vitro* methods were used to assess potential off-target activity of siRNA antisense sequence. The antisense sequence was queried against human transcriptome in NCBI BLAST. Genes were filtered according to the following criteria: 1. At most one mismatch in seed region was allowed; 2. Gene expression in liver was higher than 1 transcript per million (TPM) (HPA RNA-seq dataset, <https://www.proteinatlas.org/>). Off-target inhibitions were detected in hepG2.2.15 cells by RT-qPCR. Briefly, siRNAs were transfected to hepG2.2.15 cells at the concentration of 30, 6, 1.2, 0.24 and 0.048 nM, respectively. Total RNA was extracted at 48 h post-transfection using RNeasy Mini kit (QIAGEN) and reverse transcribed into cDNA using HiScript III RT SuperMix (Vazyme). QPCRs were performed using Sensi FAST SYBR Hi-ROX Kit (Meridian) with primers listed in Supplementary Table 5. GAPDH was used for normalization.

Animals

RAAV-HBV-B, -C, and -D mice were respectively established by intravenous injection of 1×10^{11} GC of corresponding vectors (PackGene) to C57BL/6 mice (male, 6 weeks old). RAAV-HBV-D mice with high HBsAg baseline were established by intravenous injection of 1×10^{10} vg of another rAAV-HBV vector (BrainVTA) to C57BL/6 mice (6 weeks old). All rAAV-HBV mice were kept in Jennio Biotech Co. Ltd. (Guangzhou, China). The HBV-transgenic mice C57BL/6N-Tg(1.28HBV)/Vst mice (male and female, 8-10 weeks old) with 1.28 copies of HBV genome (genotype A) were provided and kept in Vitalstar Biotechnology Co. Ltd. (Beijing, China). SD rats (male and female, 5–8 weeks old) were purchased from Vital River Laboratory Animal Technology Co., Ltd. (Chengdu, China) and maintained in WuXi AppTec (Chengdu, China) or Pharmaron (Beijing) TSP (Beijing, China). Cynomolgus monkeys (male and female, 3–4 years old) were purchased from and kept in Pharmaron (Beijing) TSP (Beijing, China). Animals were housed on a 12 light /12 dark cycle, at ~18 - 26 °C with 30 - 70% humidity.

Antiviral activity evaluation in rAAV-HBV mice and HBV-transgenic mice

RAAV-HBV-B, -C, and -D mice and HBV-transgenic mice were randomly allocated into indicated groups (6-12 mice per group) with comparable HBsAg, HBeAg and HBV DNA levels. SiRNA agents were subcutaneously injected into the mice according to specific dosage regimes. Elebsiran was served as positive control throughout the studies. Bepirovirsen and ETV were also served as positive controls in some embodiments. PBS vehicles were served as negative controls. Blood samples were collected weekly and plasma parameters including HBsAg, HBeAg, HBV DNA,

HBsAb and ALT were analyzed in HUAYIN Medical Laboratory Center. Co., Ltd. (Guangzhou, China) or DIAN Medical Testing Laboratory. Co., Ltd. (Beijing, China).

The plasma levels of HBsAg, HBeAg, and HBsAb were quantified using CLIA assay kits on Alinity i system (Abbott) or Maccura I3000 Analyzer (Maccura), with data acquired by Alinity ci-series 3.6.0 or Maccura I3000 Analyzer 1.0.11.240227. The plasma levels of HBV DNA were quantified using PCR-fluorescence probing assay kit (Sansure Biotech) on 7500 Real-Time PCR System (ABI) or SLAN automated PCR analysis system (Fosun), with data acquired by 7500 Software 2.4 or SLAN Analysis Software 8.2.2. The plasma levels of ALT were quantified by an enzymatic method with alanine aminotransferase detection kits (Zybio) on Mindray BS-2000M Automatic Biochemical Analyzer or LAbOSPECT 008AS analyzer (Hitachi), with data acquired by the instrument's native software (Immunoassay Operating Software 10.00.36.043193 or Hitachi 008AS Operating Software 1-32).

For measurement of intrahepatic HBV RNA levels, total 50 mg liver tissue was snap frozen in liquid nitrogen and ground into powder. Total RNA was extracted with RNAPrep Pure Animal Tissue Total RNA Extraction Kit (TIANGEN) and reverse transcribed into cDNA using GoScript Reverse Transcription Mix (Promega). QPCRs were performed using GoTaq qPCR Master Mix (Promega) with primers listed in Supplementary Table 5. GAPDH was used for normalization.

In certain embodiment, rAAV-HBV-D mice receiving KC13-M2G1 treatment were hydrodynamically injected with 8 µg pAAV-HBV1.2 plasmids (Fenghui) on day 60 to evaluate the protection from HBV re-exposure.

Isolation of splenocytes and liver-associated lymphocytes

In certain embodiment, rAAV-HBV-D mice receiving KC13-M1G1 were sacrificed on day 56. Spleen and liver samples were collected for HBsAg-specific B and T Cell Enzyme-linked immunospot assay (Elispot) assay. Splenocytes and liver-associated lymphocytes were isolated^{48,49}. Briefly, spleen tissues were grinded gently and washed through 70-μm sterile cell strainers (Corning). Cells were washed and resuspended in Red Blood Cells Lysis Buffer (Coolaber) to remove red blood cells. Cells were finally resuspended in fresh RPMI-1640 medium for subsequent experiments. Livers were *in situ* perfused and digested with pronase/collagenase solution (Coolaber) carefully. The cell suspensions were then filtered through a 70-μm sterile cell strainers and washed to remove excess digestion enzymes. Subsequently, cell suspensions were resuspended in Ficoll Histopaque (Solarbio) followed by density gradient centrifugation to obtain liver-associated lymphocytes. The cells were finally resuspended in fresh RPMI-1640 medium for subsequent experiments.

Enzyme-linked immunospot assay (ELISpot)

For B cell ELISpot, splenocytes were cultured in complete RPMI-1640 medium with 10% FBS containing R848 (1 μg/mL) and recombinant IL2 (10 ng/mL, Mabtech) at 37°C for 3 days and transferred to HBsAg (15 μg/mL) -coated ELISpot plates (1.0×10^5 cells/well) for additional 24-h incubation. The plates coated with 30 μg/mL anti-mouse IgG (Mabtech) and PBS were respectively served as positive and negative controls. HBsAg-specific IgG were subsequently

detected using biotinylated anti-mouse IgG and streptavidin-ALP according to the manuals (Mabtech).

For T cell ELISpot, the peptides pool containing 98 overlapped 15-mer peptides spanning the entire large surface protein was used as stimulator. The splenocytes and liver-associated lymphocytes (2.5×10^5 cells/well) were incubated in 100 μL complete RPMI-1640 medium containing 7.5 $\mu\text{g}/\text{mL}$ peptides pool in the IFN- γ , IL-2 or TNF- α Elispot plate (Mabtech) for 20 h at 37 °C. The splenocytes stimulated with combination of PMA (50 ng/mL) and ionomycin calcium (1 $\mu\text{g}/\text{mL}$) was served as positive control, and PBS stimulator was served as negative control. Spot measurement and analysis were conducted on a Mabtech IRIS 2 reader, with data acquired and processed by the Mabtech IRIS software 9.15.x.

Toxicity study in SD rats and cynomolgus monkeys

SD rats were randomly allocated into indicated groups with 6 animals per group (half males and half females). SiRNAs were subcutaneously injected into the rats once every two weeks for 4 consecutive weeks (on day 0, 14 and 28), at the doses of 50 and 200 mg/kg with a dose volume of 5 mL/kg. Clinical observation was performed every two days. Food consumption and body weight were detected twice a week. Blood samples were collected on day 15 and 29 and urine samples were collected on day 29. Clinical chemistry and hematology were measured by Hitachi 7180 analyzer with data acquired by Hitachi 7180 analyzer-7186079-06. Urinalysis was performed by CLINITEK Novus automated urine chemistry analyzer (Siemens Healthineers) with data acquired by CLINITEK Novus software S003785 1.3.6.0. Gross pathology and microscopic observation

were performed at the terminal sacrifice (on day 29). Livers, kidneys and injection sites from study animals were embedded in paraffin, sectioned, stained with H&E and microscopically evaluated. Histopathology grades were assigned as minimal (1), mild (2), moderate (3), and severe (4). Histopathologic evaluation was performed by at least two experienced pathologists in a blinded manner. The histopathology figures were acquired by NanoZoomer 2.0-RS C10730-12 Scanner (Hamamatsu) with software NDP. scan 3.1.

Cynomolgus monkeys were also randomly allocated into indicated groups with 10 animals per group (half males and half females). SiRNAs were subcutaneously injected into the monkeys once every two weeks for 4 consecutive weeks (on day 0, 14 and 28), at the doses of 30, 100 and 200 mg/kg with a dose volume of 2 mL/kg. The parameters evaluated were similar to that in rats, including mortality, clinical observations, body weights, food consumption, clinical pathology (clinical chemistry, hematology, coagulation and urinalysis), macroscopic, and microscopic pathology.

Immunogenicity study of KC13-M2G2 in SD rats and cynomolgus monkeys

SD rats were randomly allocated into indicated groups with 10 animals per group (half males and half females). KC13-M2G2 was administered repeatedly via subcutaneous injection to SD rats at 25, 50 or 100 mg/kg once every two weeks for 4 consecutive weeks (on day 0, 14, and 28) with an 8-week recovery period. Serum cytokine levels (including IL-2, IL-6, IL-10, TNF- α and IFN- γ) were assayed 4 h after the first dose and the final dose (Day 0-4 h and Day 28-4 h), 24 h after the first dose and the final dose (Day 1 and Day 29) and at the study terminus (Day 85), using Rat

Luminex Discovery Assay (R&D) on Luminex 200 analyzer, with data acquired by Luminex 200 xPONENT 4.3.1. Serum lymphocyte profiles were detected on day 1, day 29 and day 85, employing an immunophenotyping panel to assess the percentages and absolute numbers of lymphocyte subpopulations of total T cells ($CD45^+ CD3^+$), helper T cells ($CD45^+ CD3^+ CD4^+ CD8^-$) and cytotoxic T cells ($CD45^+ CD3^+ CD4^- CD8^+$) on flow cytometry (FACS Canto II, BD), with data acquired by SAS 9.4 for Windows. Briefly, the blood samples were washed with DPBS and subsequently incubated with pre-mixed antibody for 30 min at room temperature on an orbital shaker. FACS Lysing Solution (diluted 1:10 using deionized water) was added to each sample and incubated for additional 10 min. The samples were subsequently washed with DPBS and resuspended in DPBS for analysis on flow cytometer.

Cynomolgus monkeys were also randomly allocated into indicated groups with 10 animals per group (half males and half females). Similar parameters were investigated in cynomolgus monkeys after three doses of 30, 100, or 200 mg/kg administered on day 0, 14, and 28, with an 8-week recovery period. Serum cytokine levels (including IL-2, IL-6, IL-10, TNF- α and IFN- γ) in monkeys were assessed at the same timepoint as in SD rats, using NHP XL Cytokine Luminex Performance Premixed Kit (R&D) according to the manufacturer's protocols. Serum lymphocyte profiles were detected as described above. Details of the antibodies and their dilutions are provided in Supplementary Table 6.

The gating strategy was performed as follows: Lymphocytes were identified based on CD45 positivity and side scatter (SSC). Approximately 11,000 events were collected within this gate.

Total T cells were then defined as CD45⁺ CD3⁺ events, listed in the lower right quadrant (Q4) gate of the 2-parameter (CD3 vs. SSC) dot plot gated on lymphocytes. Helper T cells were defined as CD45⁺ CD3⁺ CD4⁺ CD8⁻ events, listed in the lower right quadrant (Q4) gate of the 2-parameter (CD4 vs. CD8) dot plot gated on CD45⁺ CD3⁺ cells. Cytotoxic T cells were defined as CD45⁺ CD3⁺ CD4⁺ CD8⁺ events, listed in the upper left quadrant (Q4) gate of the 2-parameter (CD4 vs. CD8) dot plot gated on CD45⁺ CD3⁺ cells. Figures exemplifying the gating strategy are provided in Supplementary Figs. 16 and 17.

Statistical analysis

The data are expressed as mean ± SD or mean ± SEM, as indicated in figure legends. Data were analyzed using one-way ANOVA with Dunn's post-hoc test. Prior to conducting parametric tests, all data were assessed for normality. When the assumption of normal distribution was violated, non-parametric test Kruskal-Wallis with Dunn's post-hoc test was employed. The specific statistical methods are indicated in the figure legends. Only statistically significant differences are indicated.

Data availability

All data that support the findings of this study are provided in the Source Data file.

References

- 1 Hsu, Y.-C., Huang, D. Q. & Nguyen, M. H. Global burden of hepatitis B virus: current

- status, missed opportunities and a call for action. *Nat. Rev. Gastroenterol Hepatol.* **20**, 524-537 (2023).
- 2 Thomas, D. L. & Longo, D. L. Global elimination of chronic hepatitis. *N. Engl. J. Med.* **380**, 2041-2050 (2019).
- 3 Wiktor, S. Z. & Hutin, Y. J. F. The global burden of viral hepatitis: better estimates to guide hepatitis elimination efforts. *Lancet* **388**, 1030-1031 (2016).
- 4 Tong, S. & Revill, P. Overview of hepatitis B viral replication and genetic variability. *J. Hepatol.* **64**, S4-S16 (2016).
- 5 Tsai, K.-N., Kuo, C.-F. & Ou, J.-H. J. Mechanisms of hepatitis B virus persistence. *Trends Microbiol.* **26**, 33-42 (2018).
- 6 Dusheiko, G., Longo, D. L., Agarwal, K. & Maini, M. K. New approaches to chronic hepatitis B. *N. Engl. J. Med.* **388**, 55-69 (2023).
- 7 Wooddell, C. I. *et al.* RNAi-based treatment of chronically infected patients and chimpanzees reveals that integrated hepatitis B virus DNA is a source of HBsAg. *Sci. Transl. Med.* **9** (2017).
- 8 Wang, X. *et al.* Dysregulated response of follicular helper T cells to hepatitis B surface antigen promotes HBV persistence in mice and associates with outcomes of patients. *Gastroenterology* **154**, 2222-2236 (2018).
- 9 Heim, K. *et al.* Attenuated effector T cells are linked to control of chronic HBV infection. *Nat. Immunol.* **25**, 1650-1662 (2024).
- 10 Burton, A. R. *et al.* Circulating and intrahepatic antiviral B cells are defective in hepatitis

- B. J. Clin. Invest. **128**, 4588-4603 (2018).
- 11 Maini, M. K. & Pallett, L. J. Defective T-cell immunity in hepatitis B virus infection: why therapeutic vaccination needs a helping hand. *Lancet Gastroenterol. Hepatol.* **3**, 192-202 (2018).
- 12 Wu, D. *et al.* Update on the treatment navigation for functional cure of chronic hepatitis B: expert consensus 2.0. *Clin. Mol. Hepatol.* **31**, S134-S164 (2025).
- 13 Moini, M., & Fung, S. HBsAg loss as a treatment endpoint for chronic HBV infection: HBV cure. *Viruses* **14**, 657 (2022).
- 14 Organization, W. H. Guidelines for the prevention, diagnosis, care and treatment for people with chronic hepatitis B infection (text extract): executive summary. *Infect. Dis. Immun.* **4**, 103-105 (2024).
- 15 Wong, G. L. H. Updated guidelines for the prevention and management of chronic hepatitis B—World Health Organization 2024 compared with China 2022 HBV guidelines. *J. Viral Hepat.* **31**, 13-22 (2024).
- 16 Jiang, P. *et al.* Single-cell RNA sequencing reveals the immunoregulatory roles of PegIFN- α in patients with chronic hepatitis B. *Hepatology* **79**, 167-182 (2024).
- 17 Rijckborst, V. & Janssen, H. L. The role of interferon in hepatitis B therapy. *Curr. Hepat. Rep.* **9**, 231-238 (2010).
- 18 Wang, F.-S., Li, J. & Zhang, C. Why is the functional cure rate of young children with chronic hepatitis B receiving antiviral therapy considerably high? *Hepatol. Int.* **18**, 296-298 (2023).

- 19 Zeng, Q. L. *et al.* Functional cure induced by tenofovir alafenamide plus peginterferon-alpha-2b in young children with chronic hepatitis B: a case series study. *BMC Infect. Dis.* **24**, 830 (2024).
- 20 Yuen, M.-F. *et al.* VIR-2218 (elebsiran) plus pegylated interferon-alfa-2a in participants with chronic hepatitis B virus infection: a phase 2 study. *Lancet Gastroenterol. Hepatol.* **9**, 1121-1132 (2024).
- 21 Yuen, M. F. *et al.* Imdusiran (AB-729) administered every 8 weeks in combination with 24 weeks of pegylated interferon alfa-2a in virally suppressed, HBeAg-negative subjects with chronic HBV infection leads to HBsAg loss in some subjects at end of IFN treatment. *J. Hepatol.* **80**, S809-S810 (2024).
- 22 Hou, J. L. *et al.* Efficacy and safety of xalnésiran with and without an immunomodulator in virologically suppressed participants with chronic hepatitis B: End of study results from the phase 2, randomized, controlled, adaptive, open-label platform study (Piranga). *J. Hepatol.* **80**, S26 (2024).
- 23 Agarwal, K. *et al.* JNJ-73763989 and bersacapavir treatment in nucleos(t)ide analogue-suppressed patients with chronic hepatitis B: REEF-2. *J. Hepatol.* **81**, 404-414 (2024).
- 24 Yuen, M. F. *et al.* Efficacy and safety of bepirovirsen in chronic hepatitis B infection. *N. Engl. J. Med.* **387**, 1957-1968 (2022).
- 25 Huang, Z. A. *et al.* Design, pharmacology, and toxicology of a novel chemically modified siRNA targeting hepatic angiotensinogen. *Mol. Ther. Nucleic Acids.* **36**, 102542 (2025).
- 26 Sells, M. A., Chen, M. L. & Acs, G. Production of hepatitis B virus particles in Hep G2

- cells transfected with cloned hepatitis B virus DNA. *Proc. Natl. Acad. Sci. U.S.A.* **84**, 1005-1009 (1987).
- 27 Hayer, J. *et al.* HBVdb: a knowledge database for Hepatitis B Virus. *Nucleic Acids Res.* **D566-D570** (2013).
- 28 Velkov, S., Ott, J. J., Protzer, U. & Michler, T. The global hepatitis B virus genotype distribution approximated from available genotyping data. *Genes* **9** (2018).
- 29 Jackson, A. L. *et al.* Widespread siRNA “off-target” transcript silencing mediated by seed region sequence complementarity. *RNA* **12**, 1179-1187 (2006).
- 30 Lin, X. siRNA-mediated off-target gene silencing triggered by a 7 nt complementation. *Nucleic Acids Res.* **33**, 4527-4535 (2005).
- 31 Nomura, K. *et al.* Synthesis of 2'-formamidonucleoside phosphoramidites for suppressing the seed-based off-target effects of siRNAs. *Nucleic Acids Res.* **52**, 10754-10774 (2024).
- 32 Huang, L. R., Wu, H. L., Chen, P. J. & Chen, D. S. An immunocompetent mouse model for the tolerance of human chronic hepatitis B virus infection. *Proc. Natl. Acad. Sci. U.S.A.* **103**, 17862-17867 (2006).
- 33 Guidotti, L. G., Matzke, B., Schaller, H. & Chisari, F. V. High-level hepatitis B virus replication in transgenic mice. *J. Virol.* **69**, 6158-6169 (1995).
- 34 Ji, Y. *et al.* The impact of hepatitis B surface antigen reduction via small interfering RNA treatment on aatural and vaccine (BRII-179)-induced hepatitis B vaccine-specific humoral and cellular immune responses. *Gastroenterology*. S0016-5085(25)00466-4 (2025).
- 35 Iwakawa, H. O., & Tomari, Y. Life of RISC: Formation, action, and degradation of RNA-

- induced silencing complex. *Mol. Cell.* **82**, 30–43 (2022).
- 36 Wong, G. L. H., Gane, E., & Lok, A. S. F. How to achieve functional cure of HBV: Stopping NUCs, adding interferon or new drug development?. *J Hepatol.* **76**, 1249–1262 (2022).
- 37 Pootier, D. D. *et al.* mRNA Therapeutic Vaccine for Hepatitis B Demonstrates Immunogenicity and Efficacy in the AAV-HBV Mouse Model. *Vaccines (Basel)* **12**, 237 (2024).
- 38 Su J. P. *et al.* Activation of CD4 T cells during prime immunization determines the success of a therapeutic hepatitis B vaccine in HBV-carrier mouse models. *J. Hepatol.* **78**, 717-730 (2023).
- 39 Ganchua, S. C. *et al.* Reduction of hepatitis B surface antigen mediated by RNA interference therapeutic AB-729 in chronic hepatitis B patients is associated with T cell activation and a decline in exhausted CD8 T cells. SAT397, EASL (2022).
- 40 Mak, L. Y. *et al.* Mitigation of immune dysfunction in patients with sustained suppression of hepatitis B surface antigen after siRNA treatment. OS-071, EASL (2025).
- 41 Jennifer, S. *et al.* Proteomic profiling in prefilled syringe study demonstrates bepirovirsen's immune stimulatory effect. Abstract 1139, AASLD (2025).
- 42 Andre, B. *et al.* Intrahepatic and peripheral immunophenotyping of participants with chronic hepatitis B receiving bepirovirsen in the B-fine study strongly suggests that bepirovirsen may trigger a humoral response. Abstract 1215, AASLD (2025).
- 43 Wen, X. *et al.* Robust and sustained hepatitis B surface antigen reduction after HT-101 dosed twice in chronic hepatitis B patients: results from a phase I study including extension

- follow-up data. PP0256, APASL (2025).
- 44 Zhang, Z. *et al.* Inhibition of hepatitis B virus replication by a novel GalNAc-siRNA in vivo and in vitro. *ACS omega.* **10**, 484–497 (2025).
- 45 Burwitz, B. J., Zhou, Z., Li, W. Animal models for the study of human hepatitis B and D virus infection: New insights and progress. *Antiviral Res.* **182**, 104898 (2020).
- 46 Burwitz, B. J. *et al.* Hepatocytic expression of human sodium-taurocholate cotransporting polypeptide enables hepatitis B virus infection of macaques. *Nat Commun.* **8**, 2146 (2017).
- 47 Biswas, S. *et al.* Long-term hepatitis B virus infection of rhesus macaques requires suppression of host immunity. *Nat Commun.* **13**, 2995 (2022).
- 48 Mederacke, I., Dapito, D. H., Affò, S., Uchinami, H. & Schwabe, R. F. High-yield and high-purity isolation of hepatic stellate cells from normal and fibrotic mouse livers. *Nat. Protoc.* **10**, 305-315 (2015).
- 49 Zhao, H. J. *et al.* Cholesterol accumulation on dendritic cells reverses chronic hepatitis B virus infection-induced dysfunction. *Cell Mol. Immunol.* **19**, 1347-1360 (2022).

Acknowledgements

We thank Dr. Kai Xiong for data-crosschecking and analyzing in the *in vitro* and *in vivo* efficacy study, Dr. Zhong-Cai Gao for the contributions in conducting toxicity study. We thank professor Fu-Sheng Wang of the Fifth Medical Center of Chinese PLA General Hospital for his helpful discussion and suggestion in the study. We would like to acknowledge the funding from Youcare Pharmaceutical Group Co., Ltd.

Author contributions

G.-S.S. administered and supervised the project. Z.-A.H. conceived and designed the study and revised the manuscript. Z.-A.H. and S.Y. designed the sequences, modification patterns and GalNAc delivery system. Z.-A.H., Y.Y. and S.Y. performed all the *in vitro* and *in vivo* experiments, analyzed all the data. Y.Y. drew the figures and drafted the manuscript. G.-S.J. conducted the *in silico* analysis and performed partial *in vitro* experiments. Z.-K.T., Y.-C.W. and R.F. performed all chemistry synthesis. Z.-A.H., Y.Y. and S.Y. contributed equally. All authors contributed to the scientific discussion and modified the manuscript.

Competing interests

The authors declare no competing interests.

Tables

Table 1 Conservation of KC13-M2G2 across HBV genotypes A to H.

genotype	A	B	C	D	E	F	G	H	All
% global infection ²⁸	16.9	13.5	26.1	22.1	17.6	0.86	0.04	0.07	97.2
Number of sequences analyzed ^a	1038	1922	2954	1701	353	296	41	31	8336
% core region conservation ^b	96.4	79.7	91.5	95.9	94.6	0.7	95.1	0	86.9
% seed region conservation ^c	98.4	80.9	97.0	99.4	98.9	91.6	100	96.8	93.9

^a 8336 HBV genotype A–H sequences downloaded on May 28, 2025.

^b Complete complementarity to position 2–19 of antisense strand.

^c Complete complementarity to position 2–8 of antisense strand.

Figure Legends

Fig. 1 ***In vitro* performances of KC13-M2G2 in HepG2.2.15 cells.** KC13-M2G2 and elebsiran were transfected into cells at concentrations of 10 to 0.00015 nM. The medium was replaced with fresh medium on day 3 post-transfection. On day 6 post-transfection, HBsAg (**a**), and HBeAg (**c**) in supernatants were quantified using chemiluminescence immunoassay (CLIA) commercial Kits, and HBV DNA (**b**) was quantified using HBV primers and quantitative polymerase chain reaction (qPCR). HBV S mRNA (**d**) and total RNA (**e**) in cells were detected by reverse transcription quantitative polymerase chain reaction (RT-qPCR). The primers used were listed in Supplementary Table 5. Cell viabilities (**f**) were determined using Cell Counting Kit-8 (CCK-8) according to the manuals. Data are shown as mean ± SEM (n=3 biologically independent replicates). Source data are provided as a Source Data file.

Fig. 2 **Pan-genotypic efficacy of KC13-M2G2.** HepG2 cells were transfected with 10 kinds of HBV genotype plasmids (**a-j**) on day 0 and siRNA agents on day 1. The medium was replaced with fresh medium on day 3 post-transfection. HBsAg content in supernatants were detected by CLIA commercial Kits on day 8. Data are shown as mean ± SEM (n=3 biologically independent replicates). Source data are provided as a Source Data file.

Fig. 3 **Efficacy of KC13-M2G2 in rAAV-HBV-B and -C mice at three weekly doses of 3 mg/kg.** Elebsiran served as positive control. The first dosing day was defined as D0. Plasma levels of HBsAg, HBV DNA, HBeAg, HBsAb and alanine aminotransferase (ALT) in rAAV-HBV-B mice

(**a-e**) and rAAV-HBV-C mice (**f-j**) were detected at certain timepoints. The levels of HBsAg, HBeAg, and HBsAb were quantified by CLIA assays on commercial analytical systems, HBV DNA by PCR-fluorescence probing assay, and ALT by enzymatic method. Data are shown as mean ± SEM (n=10 mice). Dashed lines indicate the lowest limit of quantifications (LLOQs). Source data are provided as a Source Data file.

Fig. 4 Efficacy of KC13-M2G2 in rAAV-HBV-D mice at three weekly doses of 0.1, 0.3, 1, or 3 mg/kg. Elebsiran, bepirovirsen and ETV served as positive controls. The first dosing day was defined as D0. Plasma levels of HBsAg (**a**), HBV DNA (**b**), HBeAg (**c**), HBsAb (**d**) and ALT (**e**) were detected at certain timepoints. The levels of HBsAg, HBeAg, and HBsAb were quantified by CLIA assays on commercial analytical systems, HBV DNA by PCR-fluorescence probing assay, and ALT by enzymatic method. Data are shown as mean ± SEM (n=10 mice). Dashed lines indicate LLOQs. Source data are provided as a Source Data file.

Fig. 5 Efficacy of KC13-M2G2 in rAAV-HBV-D mice with high HBsAg baseline at three weekly doses of 3 mg/kg. Elebsiran, bepirovirsen and ETV served as positive controls. The first dosing day was defined as D0. Plasma levels of HBsAg (**a**), HBV DNA (**b**), HBeAg (**c**), HBsAb (**d**) and ALT (**e**) were detected at certain timepoints. The levels of HBsAg, HBeAg, and HBsAb were quantified by CLIA assays on commercial analytical systems, HBV DNA by PCR-fluorescence probing assay, and ALT by enzymatic method. Data are shown as mean ± SEM (n=10 mice). Dashed lines indicate LLOQs. Source data are provided as a Source Data file.

Fig. 6 Efficacy of KC13-M2G2 in HBV-transgenic mice at three weekly doses of 0.3, 1 and 3 mg/kg. Elebsiran, bepirovirsen and ETV served as positive controls. The first dosing day was defined as D0. Plasma levels of HBsAg (**a**), HBV DNA (**b**), HBeAg (**c**), and ALT (**d**) were detected at certain timepoints. The levels of HBsAg and HBeAg were quantified by CLIA assays on commercial analytical systems, HBV DNA by PCR-fluorescence probing assay, and ALT by enzymatic method. Data are shown as mean ± SEM (n=6 mice). Dashed lines indicate LLOQs. Source data are provided as a Source Data file.

Fig. 7 Selected clinical pathology parameters and microscopic liver findings measured in rats. The rats received three repeat doses of KC13-M2G2 on day 0, 14, and 28. Elebsiran was included as a comparison. **a-e** Plasma ALT, aspartate aminotransferase (AST), total bilirubin (BIL-T), urea and alkaline phosphatase (ALP) were tested by biochemical analyzer on day 15 and 29. **f** Summary of the range of microscopic liver findings based on severity grade. Livers were harvested on day 29, and stained with hematoxylin and eosin (H&E). Histopathologic evaluation was conducted in a blinded manner by at least two experienced pathologists. Histopathology grades were assigned as minimal (1), mild (2), moderate (3), and severe (4). **g** Body weights were measured at certain timepoints, M and F indicate male and female rats, respectively. Data are shown as mean ± SEM (n=6 rats). Only statistically significant differences are indicated (one-way ANOVA test or Kruskal-Wallis test with Dunn's post-hoc test for multiple groups). Source data are provided as a Source Data file.

Fig. 8 Selected clinical pathology parameters, body weights and microscopic findings in cynomolgus monkeys. The monkeys received three repeat doses of KC13-M2G2 on day 0, 14, and 28. **a-e** Plasma ALT, aspartate aminotransferase (AST), total bilirubin (BIL-T), blood urea nitrogen (BUN) and alkaline phosphatase (ALP) were tested by biochemical analyzer on day -7 and 30. **f** Body weights were measured at certain timepoints. **g** Summary of the range of microscopic findings based on severity grade. Tissues were harvested on day 30, and stained with hematoxylin and eosin (H&E). Histopathologic evaluation was conducted in a blinded manner by at least two experienced pathologists. Histopathology grades were assigned as minimal (1), mild (2), moderate (3), and severe (4). Data are shown as mean \pm SEM ($n=10$ monkeys for **a-f**, and $n=6$ monkeys for **g**). Only statistically significant differences are indicated (one-way ANOVA test or Kruskal-Wallis test with Dunn's post-hoc test for multiple groups). Source data are provided as a Source Data file.

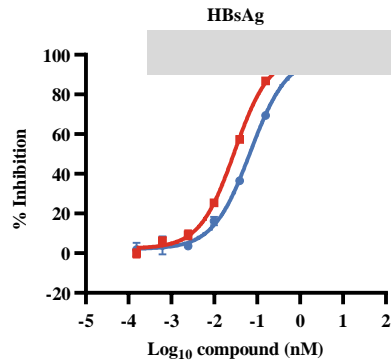
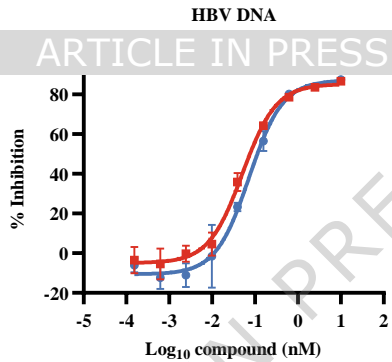
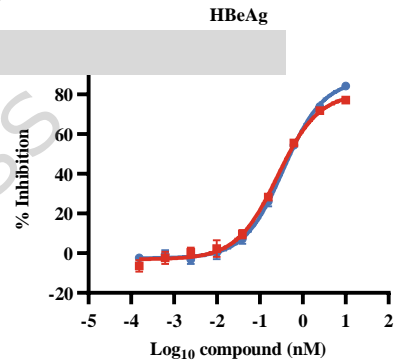
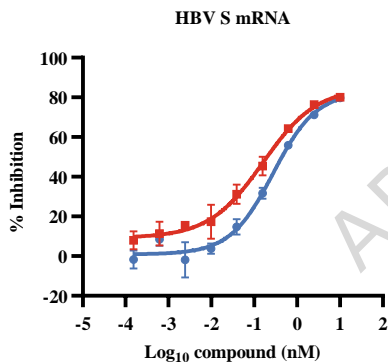
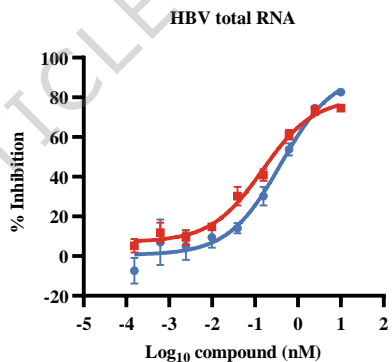
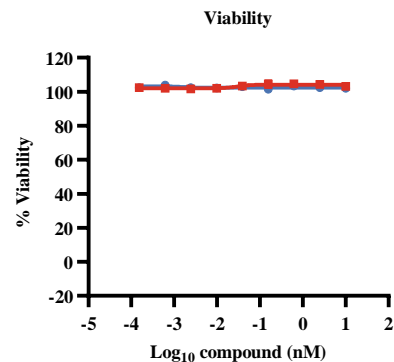
Fig. 9 Immunogenicity of KC13-M2G2 in cynomolgus monkeys. KC13-M2G2 was administered repeatedly via subcutaneous injection to cynomolgus monkeys at 30, 100 or 200 mg/kg on day 0, 14, and 28 with an 8-week recovery period. **a-e** Serum cytokine levels (including IL-2, IL-6, IL-10, TNF- α and IFN- γ) were assayed 4 h after the first dose and the final dose (Day 0-4 h and Day 28-4 h), 24 h after the first dose and the final dose (Day 1 and Day 29) and at the recovery period terminus (Day 85), using NHP XL Cytokine Luminex® Performance Premixed Kit. **f-l** Serum absolute numbers and percentages of lymphocyte subpopulations of total T cells ($CD45^+ CD3^+$), cytotoxic T cells ($CD45^+ CD3^+ CD4^- CD8^+$), and helper T cells ($CD45^+ CD3^+$

CD4⁺ CD8⁻) were detected on day 1, day 29 and day 85 by flow cytometry, employing an immunophenotyping panel. The first dosing day was defined as Day 0. Data of **a-l** are shown as mean ± SEM (n=4 monkeys for Day 85 and n=10 monkeys for the other timepoints). Dashed lines indicate LLOQs. Only statistically significant differences are indicated (one-way ANOVA test or Kruskal-Wallis test with Dunn's post-hoc test for multiple groups). Source data are provided as a Source Data file.

Editor's Summary

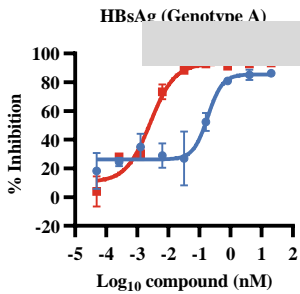
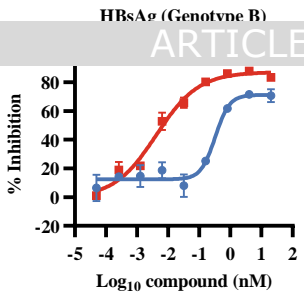
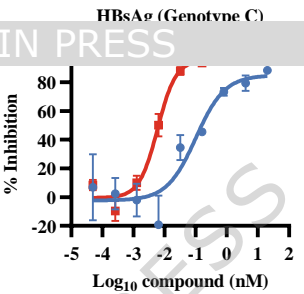
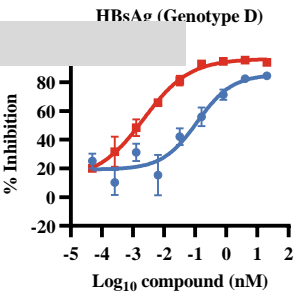
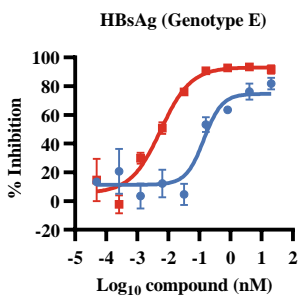
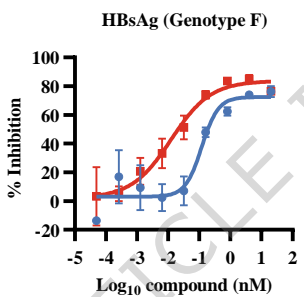
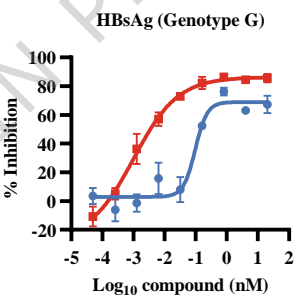
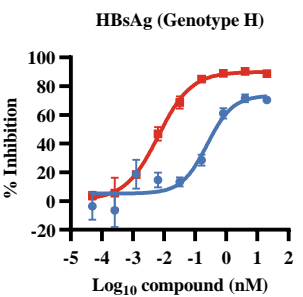
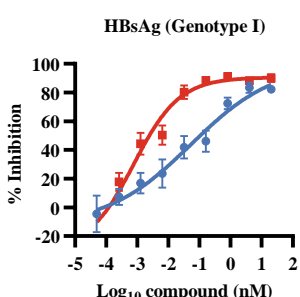
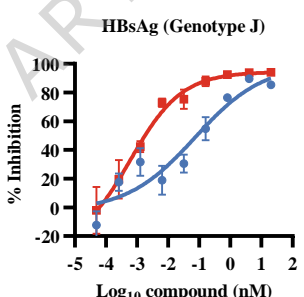
Treatments to cure chronic hepatitis B (HBV) infection are currently lacking. Here, the authors identify an HBV targeting siRNA that exhibits potent and broad-spectrum antiviral activity in preclinical animal models and demonstrates a favorable safety profile and functional cure indicators, promising clinical translation potential.

Peer review information: *Nature Communications* thanks Man-Fung Yuen, who co-reviewed with Loey Lung-Yi Mak and the other, anonymous, reviewer(s) for their contribution to the peer review of this work. A peer review file is available.

a**b****c****d****e****f**

KC13-M2G2

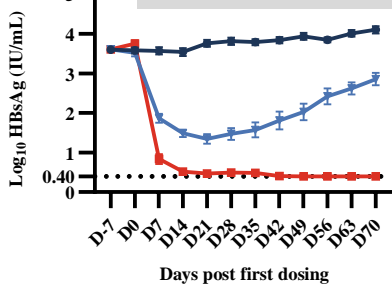
Elebsiran

a**b****c****d****e****f****g****h****i****j**

KC13-M2G2
Elebsiran

a

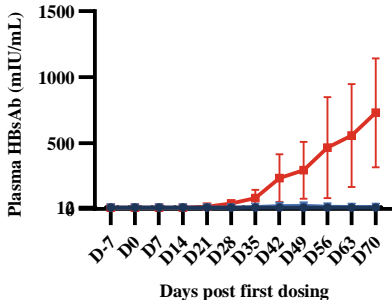
HBsAg in rAAV-HBV-B mice



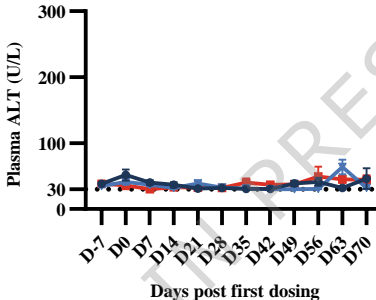
ARTICLE IN PRESS

d

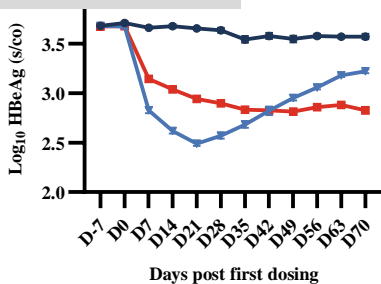
HBsAb in rAAV-HBV-B mice

**e**

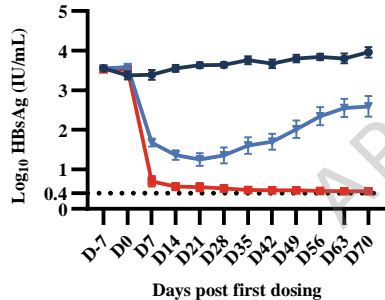
ALT in rAAV-HBV-B mice

**c**

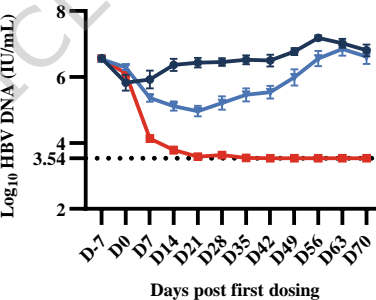
HBeAg in rAAV-HBV-B mice

**f**

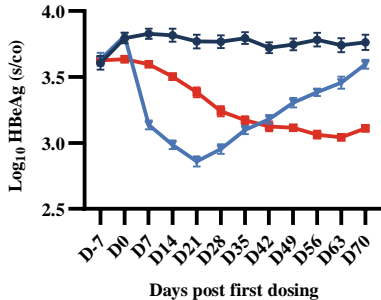
HBsAg in rAAV-HBV-C mice

**g**

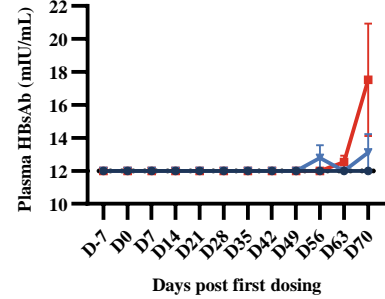
HBV DNA in rAAV-HBV-C mice

**h**

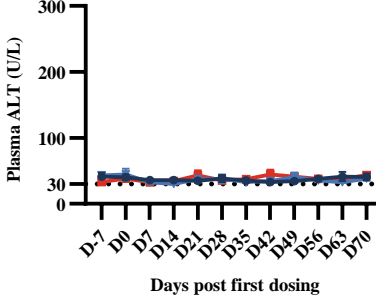
HBeAg in rAAV-HBV-C mice

**i**

HBsAb in rAAV-HBV-C mice

**j**

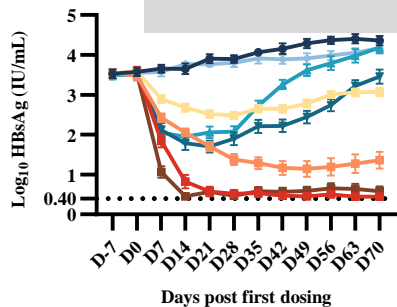
ALT in rAAV-HBV-C mice



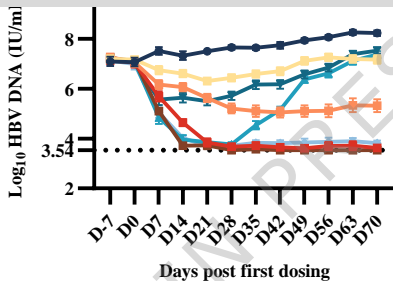
— PBS
— Elebsiran, 3 mpk, QW*3
— KC13-M2G2, 3 mpk, QW*3

a

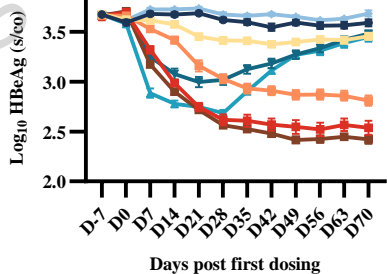
HBsAg in rAAV-HBV-D mice

**b**

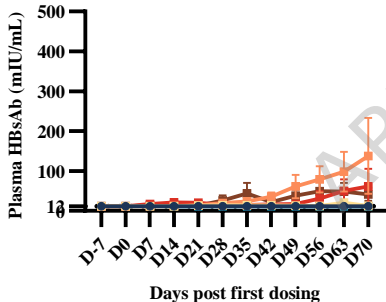
HBV DNA in rAAV-HBV-D mice

**c**

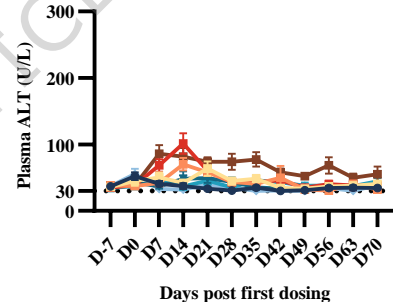
HBeAg in rAAV-HBV-D mice

**d**

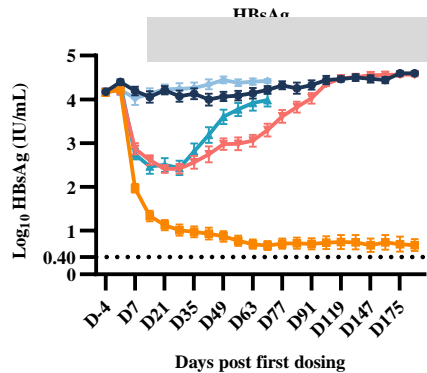
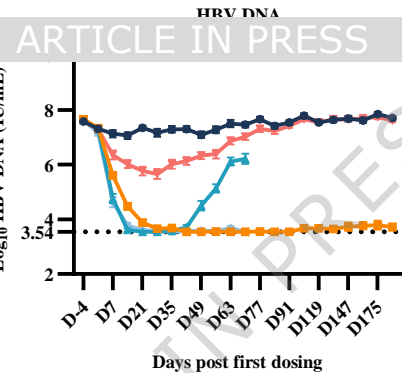
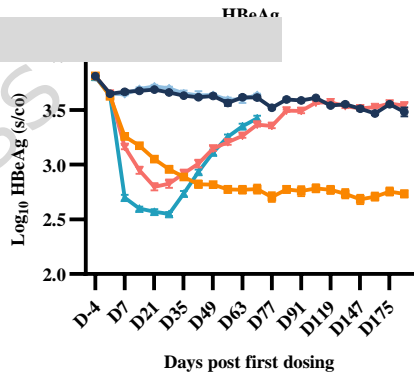
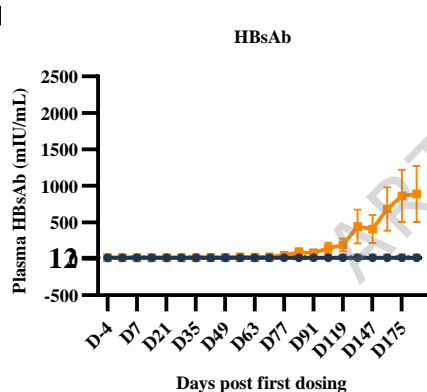
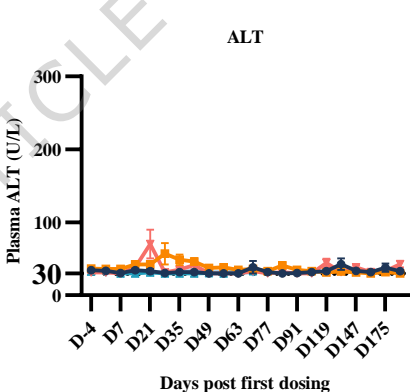
HBsAb in rAAV-HBV-D mice

**e**

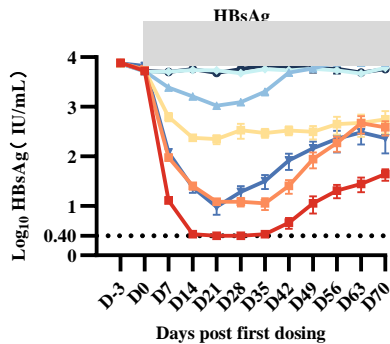
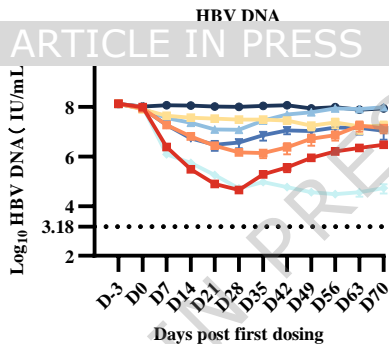
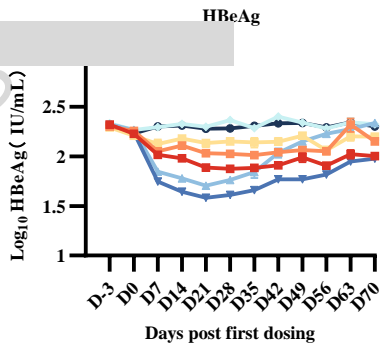
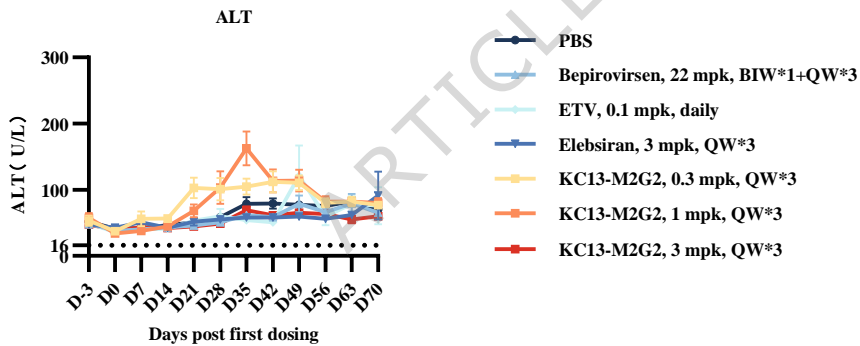
ALT in rAAV-HBV-D mice



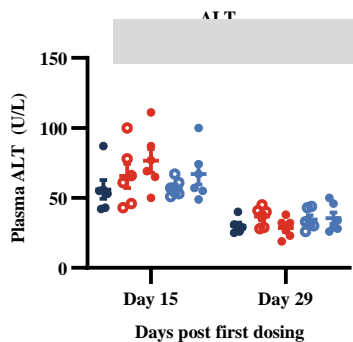
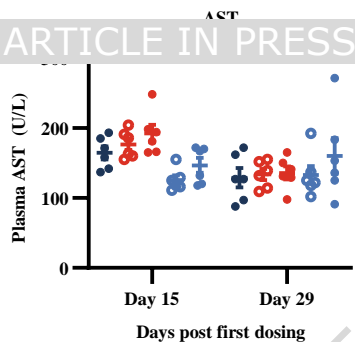
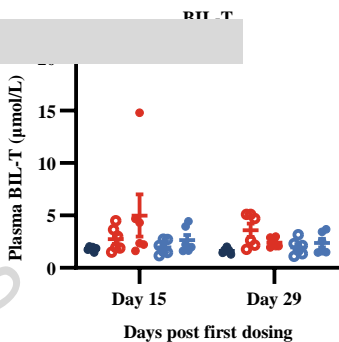
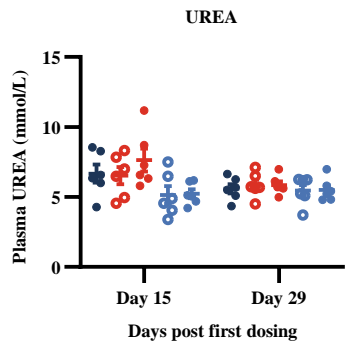
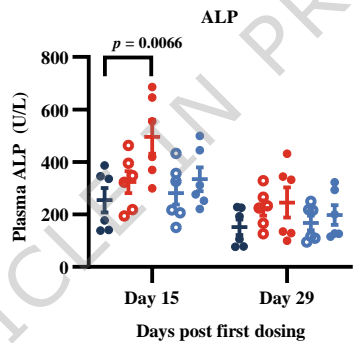
ARTICLE IN PRESS

a**b****c****d****e**

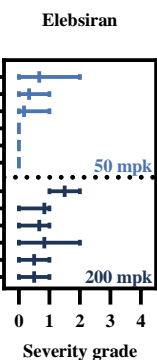
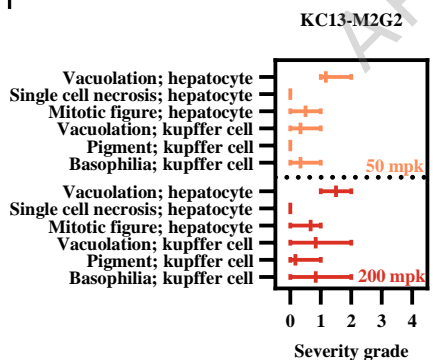
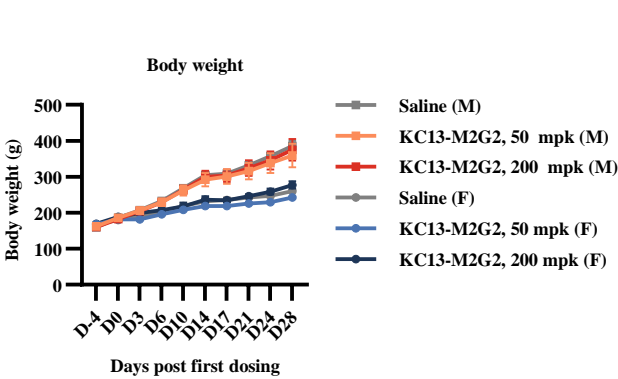
- PBS
- ▲ Bepirovirsen, 22 mpk, BIW*1+QW*3
- ◆ ETV, 0.1 mpk, daily
- Elebsiran, 3 mpk, QW*3
- KC13-M2G2, 3 mpk, QW*3

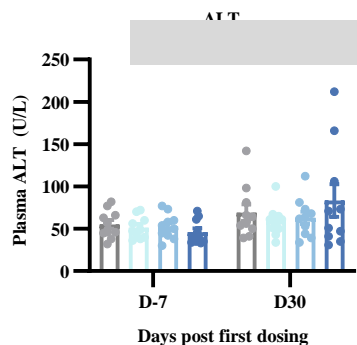
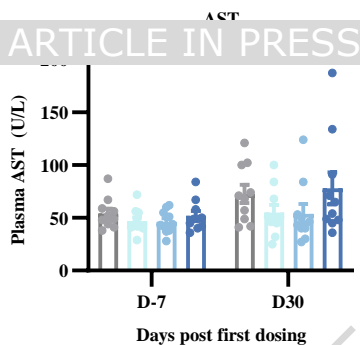
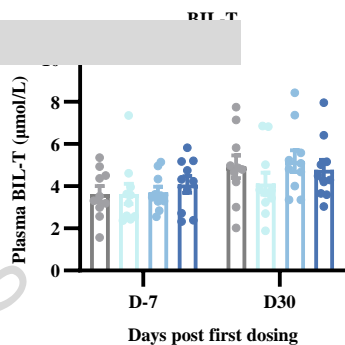
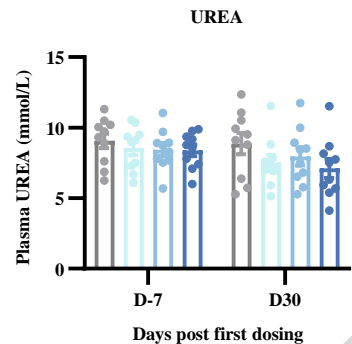
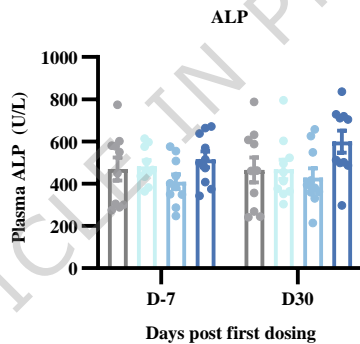
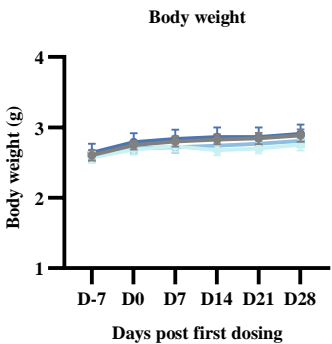
a**b****c****d**

ARTICLE IN PRESS

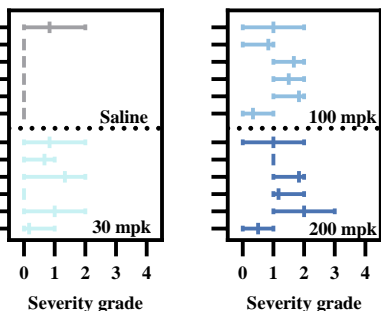
a**b****c****d****e**

- Saline
- KC13-M2G2, 50 mpk, Q2W*3
- KC13-M2G2, 200 mpk, Q2W*3
- Elebsiran, 50 mpk, Q2W*3
- Elebsiran, 200 mpk, Q2W*3

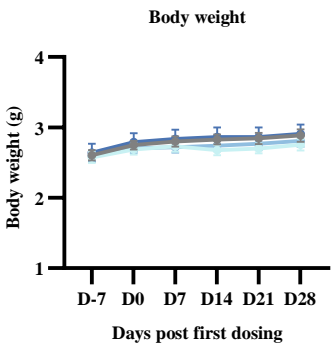
f**g**

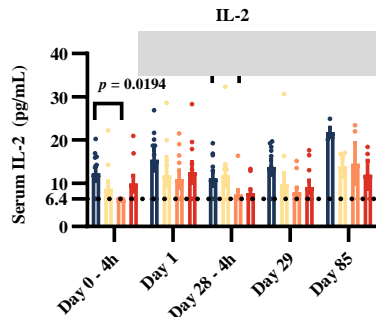
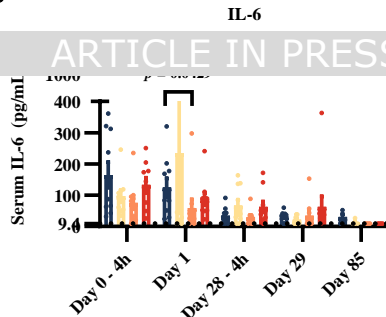
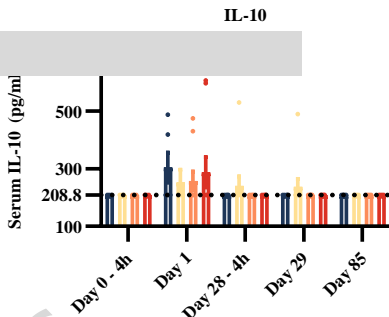
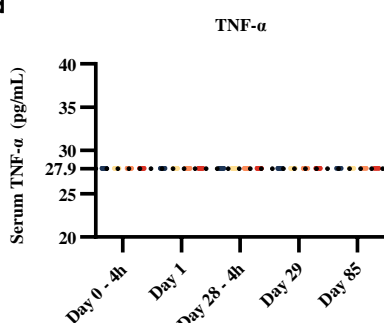
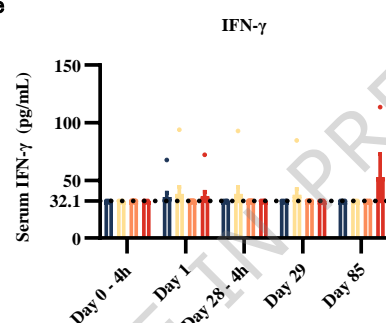
a**b****c****d****e****f****g**

- Vacuolation; hepatocyte
- Basophilia; kupffer cell
- Foamy macrophage; lymph node, mesenteric
- Foamy macrophage; lymph node, mandibular
- Foamy macrophage; lymph node, inguinal
- Basophilia; macrophage, injection site
- Vacuolation; hepatocyte
- Basophilia; kupffer cell
- Foamy macrophage; lymph node, mesenteric
- Foamy macrophage; lymph node, mandibular
- Foamy macrophage; lymph node, inguinal
- Basophilia; macrophage, injection site

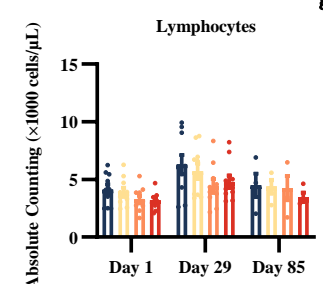
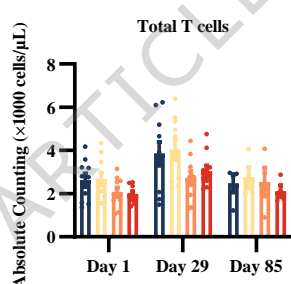
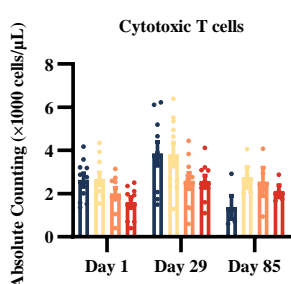
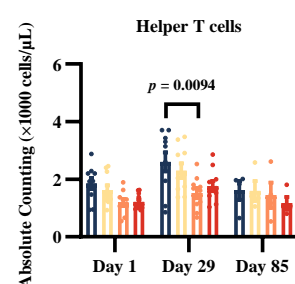
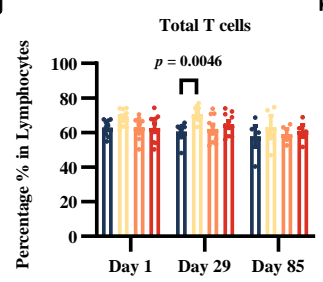
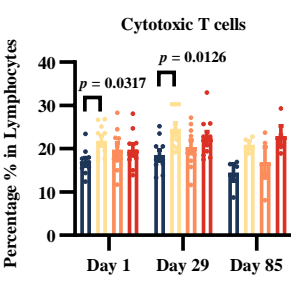
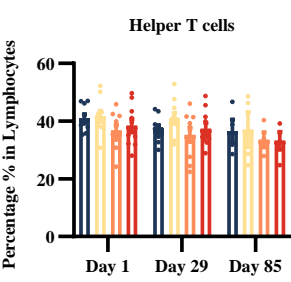


- Saline
- KC13-M2G2, 30 mpk
- KC13-M2G2, 100 mpk
- KC13-M2G2, 200 mpk

f

a**b****c****d****e**

- Saline
- KC13-M2G2, 30 mpk
- KC13-M2G2, 100 mpk
- KC13-M2G2, 200 mpk

f**g****Cytotoxic T cells****Helper T cells****h****k****Helper T cells**

- Saline
- KC13-M2G2, 30 mpk
- KC13-M2G2, 100 mpk
- KC13-M2G2, 200 mpk